Principal oscillation pattern analysis of the tropical 30- to 60-day oscillation. Part I: Definition of an index and its prediction

Article *in* Climate Dynamics · August 1990

DOI: 10.1007/BF00209520

CITATIONS
49

READS
60

2 authors, including:

Hans Von Storch
Helmholtz-Zentrum Geesthacht
506 PUBLICATIONS **17,692** CITATIONS

SEE PROFILE

Climate Dynamics (1990) 4:175–190

Climate Dynamics

Principal Oscillation Pattern analysis of the 30- to 60-day oscillation in the tropical troposphere

Part I: Definition of an index and its prediction

Hans von Storch and Jinsong Xu

Max Planck Institut für Meteorologie, Bundesstrasse 55, D-2000 Hamburg 13, Federal Republic of Germany

Received December 1, 1989/Accepted March 30, 1990

Abstract. The "Principal Oscillation Pattern" technique is used to derive an index of the 30- to 60-day oscillation in the tropical troposphere. In the 200-mb equatorial velocity potential field, one dominant pair of POPs is found. Its properties compare very well with the properties of the oscillation identified in previous studies. In particular, a good correlation between the time evolution of the POP coefficients and area-averaged outgoing long-wave radiation (ORL) is found. The POPs are derived from a 2-year subinterval of the whole 5-year data set. This leaves independent data for subsequent verification. The patterns and their characteristic numbers are almost unchanged if the whole data set is analysed. Also, the analysis is insensitive to changes of the analysis area: if the analysis is limited to 90°-longitude equatorial sectors, the signal is also identified and its patterns are consistent with the patterns derived from the full data set. Interestingly, the signal is best defined in the eastern hemisphere. The POPs may be used to derive "associated correlation patterns" of other quantities in winter and summer separately. The path of the oscillation has a marked annual cycle: in northern winter it migrates from the Indian Ocean across northern Australia into the region of the South Pacific Convergence Zone (SPCZ) and in northern summer it moves from the Indian Ocean across South Asia along the intertropical Convergence Zone (ITCZ) to South America. The POP coefficient may be seen as a bivariate index of the state (phase and strength) of the 30- to 60-day oscillation. Since the POP technique incorporates a prediction equation for the phase of the POP coefficients, the POP model allows for the prediction of the complex amplitude of the oscillation. In a sequence of forecast experiments, of which about two-thirds used independent data, the POP forecasts were found to be useful in about half of all cases for lead times of several days. The correlation and RMS skills were calculated for the POP forecast and for persistence. The POP forecast appears to be considerably better with respect to both measures. The correlation skill scores 60% after 7 days. The POP forecast is most skillful in northern winter and if strong signals are present with minima of velocity potential in the eastern hemisphere.

Offprint requests to: H von Storch

1 Introduction

The so-called 30- to 60-day oscillation, discovered by Madden and Julian in 1971, is the strongest regular tropical signal on the subseasonal time scale. Spatially, it appears mostly as a zonal oscillation number 1 pattern which travels once around the globe in 30–60 days. In the convectively active equatorial areas, the oscillation is connected with precipitation anomalies so that the oscillation may be traced by outgoing long-wave radiation (OLR).

Besides being of general academic interest, there are several aspects which make the oscillation important. The oscillation is associated with tropical weather events such as the onset and the break phases of the Indian and Australian monsoons (Hartmann and Michelsen 1989, McBride 1987). The fluctuations of the strength of the SPCZ (Huang and Vincent 1988) are probably related to the phase of the 30- to 60-day oscillation. The zonal shift of part of the tropical rainfall leads to modifications of the tropical forcing of the global atmosphere which, in turn, are connected with circulation anomalies at subtropical and mid-latitudes.

Therefore, forecasting the state of the oscillation is potentially very useful. As far as we know, no systematic study has been made as to whether the numerical weather prediction models (NWPs) currently in use are capable of predicting the oscillation adequately. One reason for this deficit is the lack of an easy-to-handle index of the oscillation.

Having previously found that the "principal oscillation patterns technique" ("POPs": Hasselmann 1988, Storch et al. 1989) is capable of identifying the 30- to 60-day oscillation in a multi-year atmospheric general circulation model (AGCM) simulation (Storch et al.

1988), we use the POPs in the present study to derive patterns that are characteristic of the real world's oscillations. The time coefficients of these patterns, i.e. the POP coefficients, are taken as a bivariate index of the oscillation. The case for doing so is justified by showing that the POP coefficients correlate well with other quantities known to reflect the 30- to 60-day oscillation, and by the fact that it is possible to infer important characteristics of the oscillation by using the coefficients as an indicator of the state of the oscillation.

One of the intriguing aspects of the POP technique is its built-in forecast ability (Xu and Storch 1990, Penland 1989). The skill of the POP forecast scheme is explored by a series of test cases, from a period not used to design the POP model, and measured by a correlation skill parameter. It must be stressed, however, that at best one can expect only a poor man's scheme that, possibly, might be run on a PC. In the long term it cannot be a serious competitor to operational NWPs. On the other hand, any NWP that claims to be skillful in predicting the oscillation has to show is superiority not only with respect to the traditional persistence but also with respect to the POP technique.

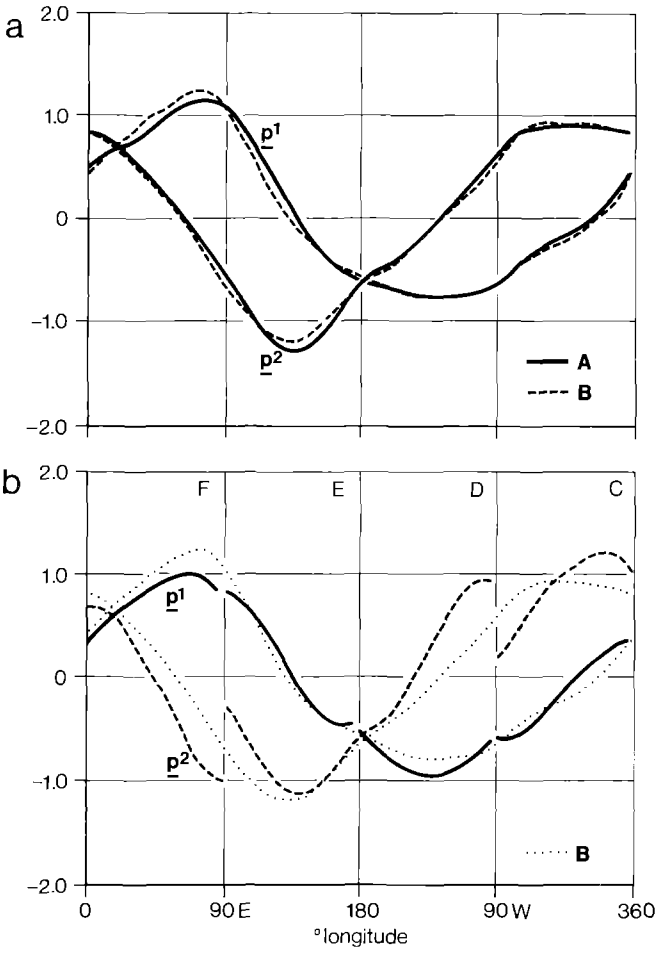

Fig. 1a, b. Principal oscillation patterns, p^1 and p^2, of equatorial 200-mbar velocity potential. The POPs tend to appear in sequences of the type $\ldots \rightarrow p^2 \rightarrow p^1 \rightarrow -p^2 \rightarrow -p^1 \rightarrow p^2 \rightarrow p^1 \rightarrow \ldots$. The POP analysis is based on daily (0 UTC) NMC analyses. Dimensionless units. **a** Analysis of equatorial data from the "analysis interval" May 1986 to April 1988 (*solid line*) and from all available data, i.e. May 1984 until April 1989 (*dashed line*). The "analysis interval" POPs are used for the associated correlation pattern analysis in Section 5, and for the predictions in Section 6 (rows A and B in Table 1). **b** Separately performed analyses for 90° longitude sectors along the equator (0°–90° E, 90° E–180°, 180°–90° W and 90° W–0°) obtained from May 1984 to April 1989 data. p^1 is given as a *solid line* and p^2 as a *dashed line*. The full 360° analysis patterns shown in Fig. 1a are indicated with *dots* for comparison. The POPs have been rotated so that p^1 fits the pattern of the 360° analysis (rows C–F in Table 1)

The purpose of the paper is to study the tropical 30- to 60-day oscillation and its predictability. The purpose is not to advocate the POP technique as a diagnostic or predictive tool. The POP, nowadays, represents a well-established technique whose suitability has been demonstrated by many applications [apart from those papers quoted above, see Latif and Villwock (1990), Penland (1989)]. A discussion of the similarity or dissimilarity of the POP technique and of the Complex EOF technique has been presented in the above referenced papers.

The paper is organized as follows. In Section 2 the data are described. In Section 3, after briefly summarizing the POP technique, the results of the POP analysis of 200-mbar equatorial velocity potential from May 1986 to April 1986 are discussed. In Section 4, the dependence of the results on the choice of analysis interval and analysis area are considered. Associated correlation patterns of tropical velocity potential and of OLR for the full year, and for winter (NDJF) and summer (MJJA), are shown in Section 5. Section 6 is devoted to the POP forecasts: the technique is outlined, several randomly chosen cases are examined in some detail and measures of skill are estimated.

2 Data

The 30- to 60-day oscillation appears in various meteorological parameters, e.g. upper-level wind and sea-level pressure (Madden and Julian 1972), velocity potential and outgoing long-wave radiation (OLR; Lau and Chan 1985, Weickmann et al. 1985), wind stress over the tropical Pacific (Madden 1988) or the length of day (Rosen and Salstein 1983, Madden 1987).

For our purposes, the upper-level velocity potential seems to be most appropriate as the signal has a smooth large-scale patterns and is global in extent. Even though the velocity potential exhibits a meridional migration in the course of the annual cycle, we anticipated that the state of the 30- to 60-day oscillation would already be well represented in the equatorial strip. We will come back to this aspect in Section 4.

Our POP analysis is therefore based on the 200-mbar velocity potential along the equator as the key variable. To gain additional insight into the structure of the oscillation, we perform an "associated correlation pattern" analysis of OLR and velocity potential at 200 mbar in the 45° N–45° S belt.

We use daily analyses (0 UTC) of NMC from May 1984 to April 1989 (Trenberth and Olson 1988). The

POP model is derived from a subset of the data, the *analysis interval* May 1986 to April 1988. The remaining *verification interval* data, from May 1984 to April 1986 and from May 1988 to April 1989, serve as independent data to evaluate the proposed forecast schemes skill. Also, in Section 4 the full data set, i.e. from the analysis interval and from the verification interval, is analysed with the POP method. This is done to examine the sensitivity of the results to the choice of the area and time interval. In all other sections, i.e. 3, 5 and 6, the POPs derived from the analysis interval are used exclusively.

For the analysis interval, daily OLR data (e.g. Liebmann et al. 1989) are available for 45° N–45° S. For a parameter that reflects the state of the oscillation, an area-averaged OLR time series is used: 5° N–5° S, 75° E–95° E is the area with a maximum of all-year intraseasonal OLR variance (Knutson et al. 1986, Weickmann et al. 1985).

The annual cycle is removed from all data by subtracting the annual and semiannual harmonic. No other time filtering was done.

3 Principal oscillation pattern analysis

3.1 Brief outline of the POP method

The "principal oscillation pattern analysis" (POP) is a statistical analysis technique to identify coherently varying patterns in a multicomponent geophysical vector time series, say $x(t)$ (Hasselmann 1988, Storch et al. 1988, 1990, Penland 1989). Its output is a set of patterns and characeristic times.

The patterns may often be grouped, as in the present case, into pairs of patterns, say p^1 and p^2. The significance of the POPs arises from the intrinsic "rotational behaviour" of these paired POPs: they tend to oscillate in a regular manner, i.e. they appear as a linear combination $z^1(t)p^1+z^2(t)p^2$ with z^1 and z^2 oscillating coherently on the "POP period" $\mathscr{T}$, and z^2 leads z^1 by about one-quarter of $\mathscr{T}$. Symbolically, this may be expressed as the system's tendency to generate sequences

$$\ldots\rightarrow p^2\rightarrow p^1\rightarrow -p^2\rightarrow -p^1\rightarrow p^2\rightarrow p^1\rightarrow\ldots$$

The period $\mathscr{T}$ is one of the characteristic numbers that is estimated by the POP analysis. Another characteristic time resulting from the POP analysis is an e-folding damping time of the POP coefficients, $z^1(t)$ and $z^2(t)$. Both characteristic numbers, the period and the e-folding damping time, describe average time scales. A full cycle $p^1\rightarrow -p^2\rightarrow -p^1\rightarrow p^2\rightarrow p^1$ will be completed in $\mathscr{T}$ on average, but some cycles may be completed in a shorter or longer time. The same holds for the e-folding damping time: in many cases a complex amplitude of length 1 will be damped to $1/e$ in that time, but there will be episodes during which disturbances are damped considerably quicker or slower.

The POP coefficients are the dot products of vectors $x(t)$ with the "adjoint POPs" p^1_A and p^2_A: $z^1(t)=x(t)\cdot p^1_A$ and $z^2(t)=x(t)\cdot p^2_A$. If we identify the POPs with a particular process, as we will do in the next sections, the process is described in a two-dimensional space which is spanned by the two POPs p^1 and p^2. The POP coefficients are the coordinates in this space, so that the state of the considered process may be represented in a z^1/z^2-dial diagram.

Mathematically, pairs of POPs form complex eigenvectors, p^1+ip^2, of the normalized lag-1 autocovariance matrix of the multivariate random variable x. As such, the POP pairs may be rotated, i.e. p^1+ip^2 may be replaced by $\alpha(p^1+ip^2)$ with any complex number α. We will use this possibility in Section 4 to allow for better comparisons between different pair of POPs.

3.2 POP analysis of 200-mbar equatorial velocity potential

When analysing the 200-mbar velocity potential with the POP technique, one physically significant pair of rotating POPs is identified. The rotation time $\mathscr{T}$ is estimated to be 44 days, and the e-folding time to be 13 days, i.e. about 30% of the rotation time (row A in Table 1). The squared coherency is larger than 68% on time scales between 20 and 50 days, with a maximum value of 96% at 50 days.

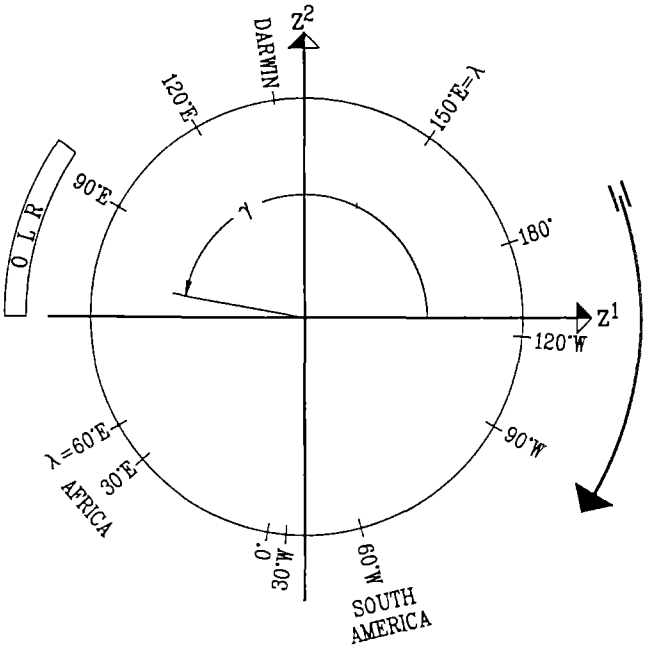

Fig. 2. Location of the miniumum λ of $\cos(\phi)p^1+\sin(\phi)p^2$ with the patterns p^1 and p^2 shown as solid lines in Fig. 1a. λ is marked on the *big circle*, and the angle ϕ is defined as the counterclockwise angle spanned by the positive z^1-axis. Note that all λs from about 60° W to 30° E are associated with very flat minima (see Fig. 1). The *big arrow* indicates the rotation direction of the POP model. The *block labelled "OLR"* indicates the longitudinal location of the OLR time series (5° N–5° S, 75° E–95° E). The angle γ is connected with maximum correlation between $\cos\gamma\cdot z^1(t)+\sin\gamma\cdot z^2(t)$ and the area-averaged OLR

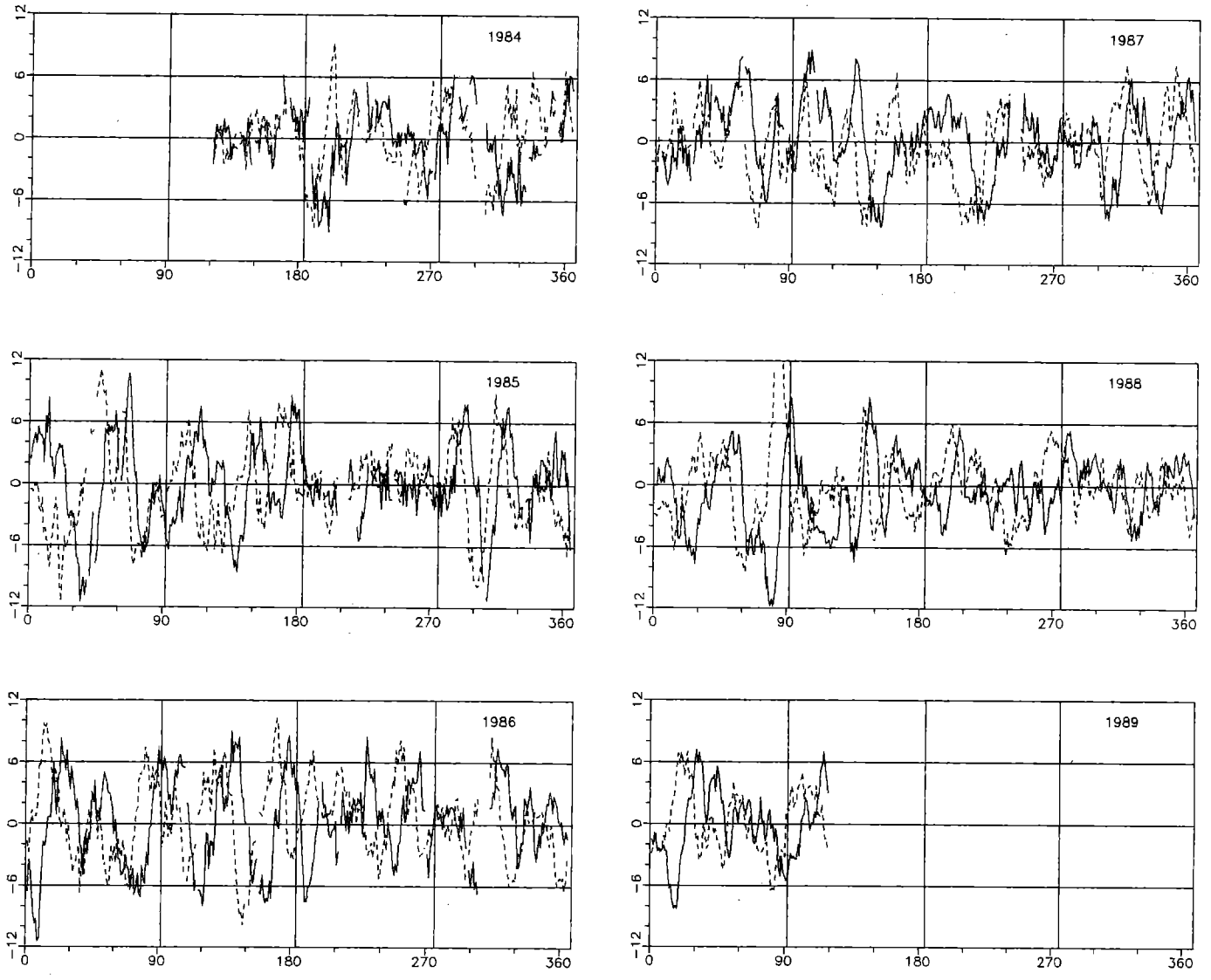

Fig. 3. Time series of POP coefficients, $z^1(t)$ (*continuous line*) and $z^2(t)$ (*dashed line*), of the solid line patterns p^1 and p^2 shown in Fig. 1a, from May 1984 until April 1989. Note that some data are missing. Units: $10^6 m^2 s^{-1}$

Some experiments were made on the preprocessing of the data, i.e. with time filtering and projection onto a low-dimensional EOF-spanned space. The results were insensitive to these details of preprocessing and it turned out that the analysis could readily be done without any time filtering of the data and by using only the first two EOFs.

The patterns p^1 and p^2 are shown as solid lines in Fig. 1. They are zonal wave number 1 type patterns with one minimum and one maximum. The two patterns are about 90° out of phase, indicating an eastward migration of the entire signal. The patterns deviate, however, in a characteristic way from a purely sinusoidal pattern; the extremes are smaller in the western than in the eastern hemisphere. More significantly, the gradients of velocity potential are strongest in the 60° E–180° sector. If, at a certain time t, the oscillation is given by $z^1(t)p^1+z^2(t)p^2$, its minimum is located at longitude λ satisfying

$$\frac{p^{2\prime}(\lambda)}{p^{1\prime}(\lambda)} = \frac{-z^1(t)}{z^2(t)} = :\tan(\phi).$$

The prime $'$ indicates a zonal derivative. In Fig. 2, the dependence of the location of the minimum, λ, on the angle $\phi = \tan^{-1}[-z/z^2]$ is shown. If the (z^1,z^2)-point spans an angle of about $\phi = 20°$ with the positive z^1-axis, the minimum is located at the dateline, i.e. $\lambda(20°) = 180°$. Similarly, $\phi = 100°$ is connected with a minimum at about Darwin longitude: $\lambda(105°) = 130°$ E. Note that the South America and Africa directions are defined rather vaguely. The propagating velocity of the crests of the "wave" clearly vary with longitude.

The time series of the POP coefficients, $z^1(t)$ and $z^2(t)$, are shown in Fig. 3. The unfiltered data are characterized by noisy high-frequency variations superimposed on coherent low-frequency oscillations. The dashed curve (z^2) leads the continuous curve (z^1) by about 10 days. The oscillation seems to be active

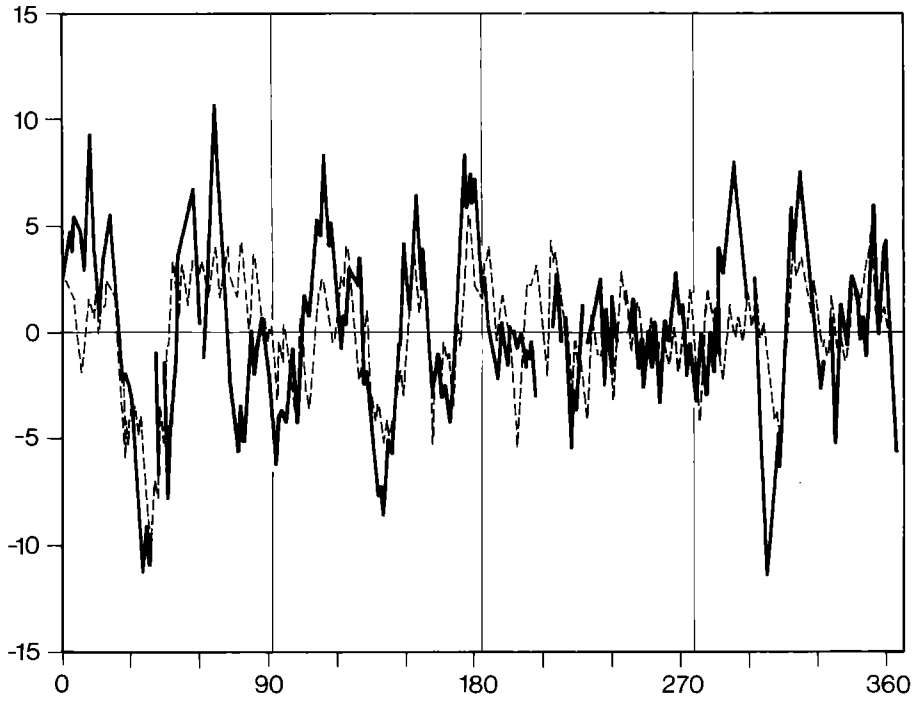

Fig. 4. Time series of POP coefficient time series $\cos\gamma \cdot z^1(t) + \sin\gamma \cdot z^2(t)$ (*continuous line*) and area-averaged OLR time series (5° N–5° S, 75° E–95° E; *dashed line*) in 1985. No filtering has been applied, apart from the removal of the first two harmonics of the annual cycle. Units: POP coefficients, $10^6 m^2 s^{-1}$; OLR, 10 Wm^{-2}. Note that the 1985 period is part of the verification interval and not of the analysis interval

throughout most of the year. There are some quiet, or less coherent, phases in late summer.

3.3 POP coefficients as an index of the tropical 30- to 60-day oscillation

The rotation period $\mathcal{T}$=44 days, the zonal wave number 1 pattern and the eastward migration of the POPs all suggest that the identified POP pair is representative of the 30- to 60-day oscillation. The characteristic deviation from a purely sinusoidal pattern has also been found previously for the 30- to 60-day oscillation (Madden and Julian 1972, Knutson and Weickmann 1987, Storch et al. 1988).

Also, the POP coefficients are well correlated with local OLR which is a good indicator of the state of the oscillation; the optimal correlation, 45%, of the time series $\cos\gamma \cdot z^1(t) + \sin\gamma \cdot z^2(t)$ and the area-averaged OLR time series (5° N–5° S, 75° E–95° E) is obtained for $\gamma = 170°$. This value is equal to ϕ(90° E). When using filtered data instead of raw data, about the same angle γ but a somewhat higher correlation is found.

The "optimal" times series, $\cos\gamma \cdot z^1(t) + \sin\gamma \cdot z^2(t)$, and the area-averaged OLR in 1985 are shown in Fig. 4: the similarity between the curves is quite remarkable. Quite clearly, the high correlation comes from the intraseasonal time scale. The same similarity is found in the other analysed years (not shown). Apparently, the POP model is quite capable of identifying the OLR anomalies related to the 30- to 60-day time scale.

Table 1. Results of the POP analysis with variable time interval and spatial domain. The number in the c^{ii} column and, for example, row F is the correlation between the *i*-th POP coefficients of the F analysis and the "B" analysis

	Time interval	Equatorial sector	Period $\mathcal{T}$ (days)	*e*-folding time (days)	c^{11} (%)	c^{22} (%)
A	May 1986–April 1988 ("analysis interval")	0°–360°	44	13	88	91
B	May 1984–April 1989 (all data)	0°–360°	43	11	100	100
C	May 1984–April 1989 (all data)	90° W–0°	42	4	65	73
D	May 1984–April 1989 (all data)	180°–90° W	33	4	76	65
E	May 1984–April 1989 (all data)	90° E–180°	61	7	79	88
F	May 1984–April 1989 (all data)	0°–90° E	42	7	88	75

It is concluded that the two POP coefficients, $z^1(t)$ and $z^2(t)$, form a bivariate index of the tropical 30- to 60 day oscillation. In Section 5, this bivariate index will be used to derive associated correlation patterns, and in Section 6 the POP forecast scheme will be used to predict the index.

4 Sensitivity of the POP analysis to the analysis area and time interval

In a series of POP analyses, denoted by "B"-"F", we tested the sensitivity of the "analysis interval" results (denoted by "A", see previous section) to changes of the analysis period and of the analysis area. This section deals only with the results of these additional analyses "B"-"F". To make the comparisons easier, all POPs are rotated so that the p^1 patterns optimally fit the "A"-p^1. This operation is not in conflict with the POP concept since pairs of POPs are defined as complex eigenvectors which may be multiplied with complex numbers.

The "A" POPs were derived from a 2-year subinterval of the entire 5-year data set (see row A of Table 1). The area considered was the entire equator, i.e. the full 0°-360° longitude sector.

2.1 Extension of analysis time interval, case B

The extension of the time interval from the "analysis interval" to the full 5-year data set is not connected with noteworthy changes of the characteristic numbers (Table 1, row B): the *e*-folding time of 11 days is sligthly smaller than in A (13 days). The B patterns shown in Fig. 1a (dashed lines) are virtually identical to the A patterns. The correlations between the B and A POP coefficient time series, which are shown for 1985 in Fig. 5, are very large (88% and 91%).

4.2 Analysis of subareas, cases C-F

In the set of analyses C-F the whole 360° equatorial

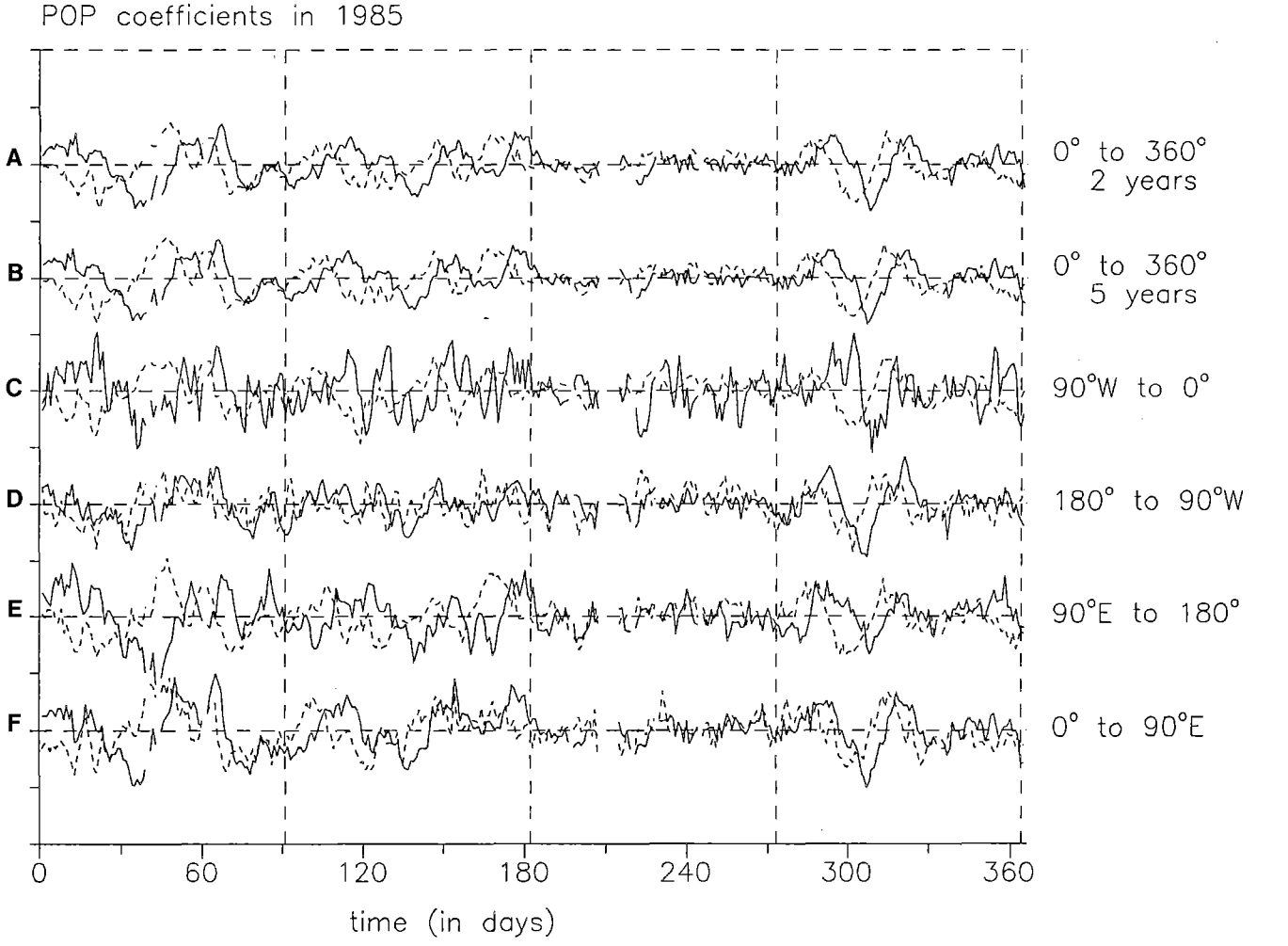

Fig. 5. Time series of coefficients, $z^1(t)$ (*continuous line*) and $z^2(t)$ (*dashed line*), of POPs derived from the analyses A-F (see Table 1), from January 1985 until December 1985. The corresponding patterns p^1 and p^2 are shown in Fig. 1. Note that some data are missing. Units: $10^6 m^2 s^{-1}$

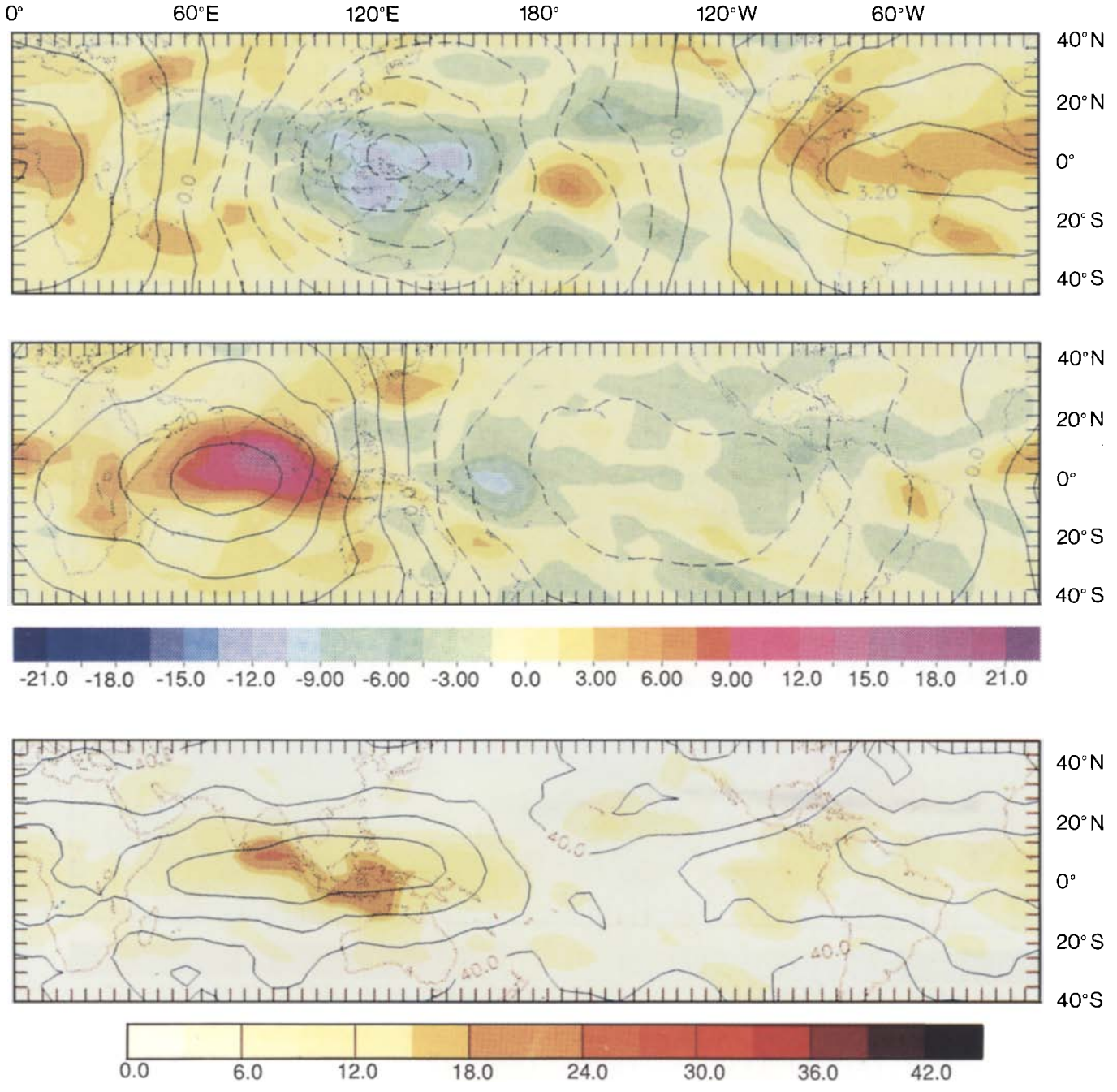

Fig. 6. Associated correlation patterns of 45° N–45° S 200-mbar velocity potential (*lines*) and of outgoing long-wave radiation (OLR; *shading*). *Top* q^2_χ and q^2_{OLR}; *middle*, q^1_χ and q^1_{OLR}; *bottom*, percentage of variance explained by POP coefficients. Units: velocity potential, $10^6 m^2 s^{-1}$; OLR, Wm^{-2}; variance, %

circle of latitude was divided into four adjacent 90° sectors. The patterns found are shown in Fig. 1b. The 90° sector patterns closely resemble the full 360° patterns. The better fit of the p^1 patterns than of the p^2 patterns is simply due to the fact that the (above-mentioned) rotation of the POPs favours the fit of the first patterns.

The characteristic numbers, listed in rows C–F of Table 1, deviate little from the 360° results given in rows A and B.

The *e*-folding times in the 90° sectors are considerably smaller than in the 360° circle. This difference is reasonable: the POPs describe a global, travelling feature which will be traced for a longer time in the 360° circle than in the 90° sectors. Interestingly, the damping time in the eastern hemisphere (E and F), 7 days, is about double that in the western hemisphere (C and D), 4 days. This finding is consistent with the observation that the 30- to 60-day oscillation is markedly stronger in the eastern hemisphere (see Section 5).

The differences in the periods in the four 90° sectors are consistent with the variable phase speed of the minimum of velocity potential depicted in Fig. 2. In the E sector 90°–180° the oscillation was found to be slowest – and the period in this sector was found to be 62 days. In the C and D sectors, 0°–90° E and 90° W–0°, the oscillation propagates with medium wave speed – and the period is 42 days. Finally, in the D sector 180°–90° W the propagation is fastest and the period is a minimum, namely 33 days. The average of the C–F periods is 45 days, i.e. almost identical to the period of the 360° analyses A and B.

The time series of 1985 are shown in Fig. 5. The eastern hemisphere sectors, E and F, yield time series very similar to cases A and B. Here the correlations between the POP coefficients are of the order of 80% (Table 1). The signals become less clear in sectors C and D, where the correlations are about 70%.

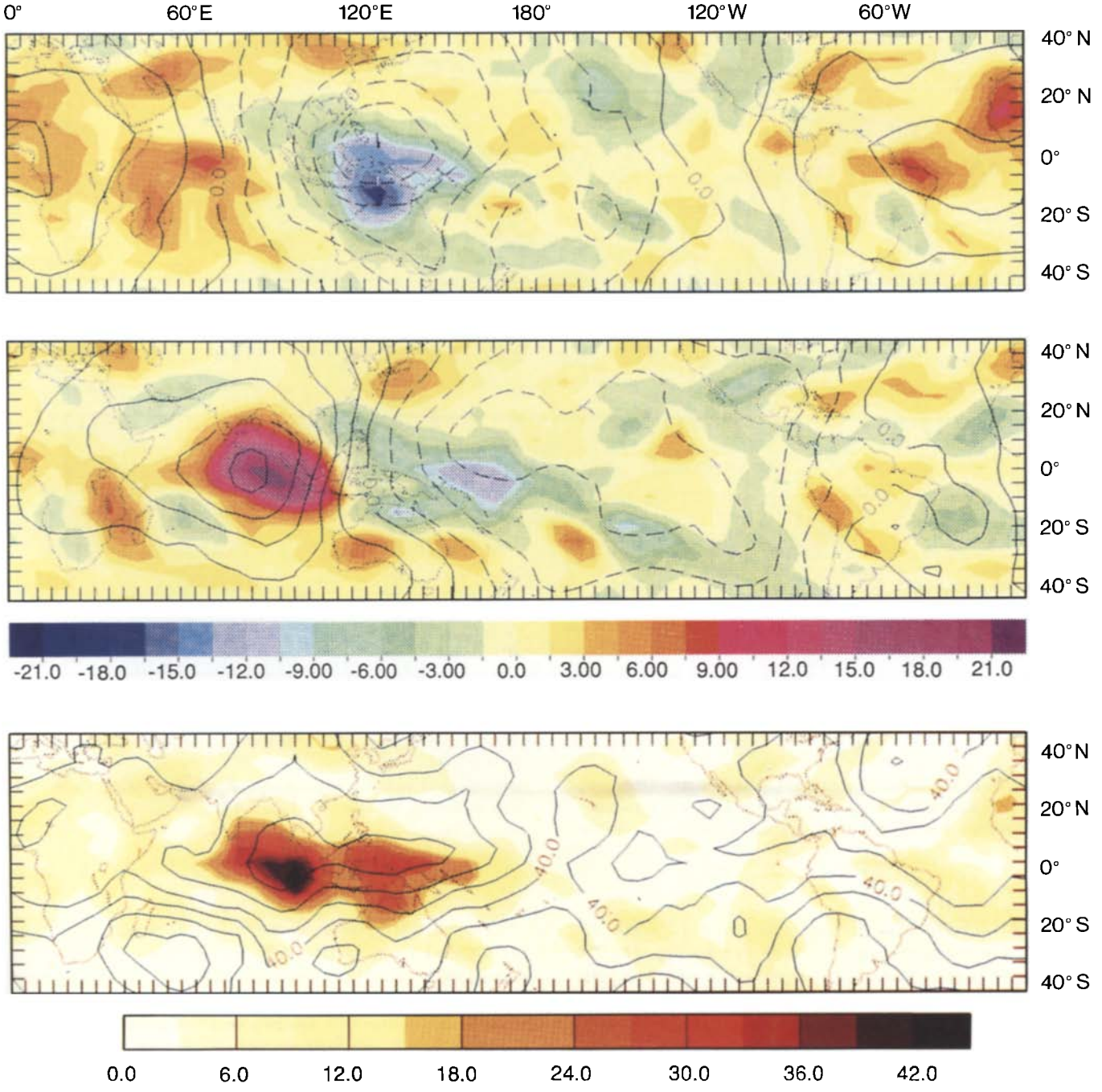

Fig. 7. Same as Fig. 6, but for northern winter (NDJF). Associated correlation patterns of 45° N–45° S 200-mbar velocity potential (*lines*) and of outgoing long-wave radiation (OLR; *shading*). *Top*, q_χ^2 and q_{OLR}^2; *middle*, q_χ^1 and q_{OLR}^1; *bottom*, percentage of variance explained by POP coefficients. Units: velocity potential, $10^6 m^2 s^{-1}$; OLR, Wm^{-2}; variance, %

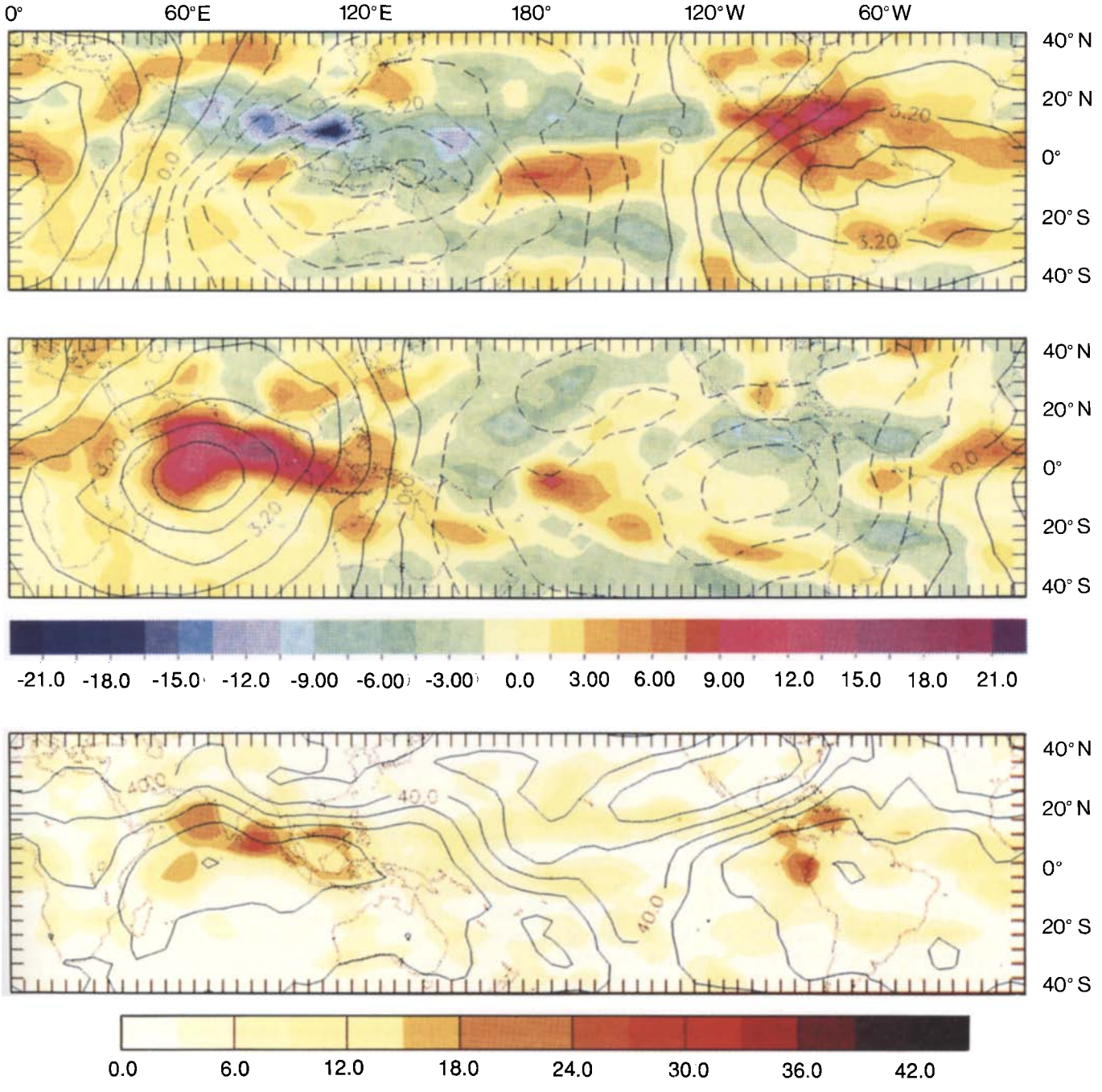

Fig. 8. Same as Fig. 6, but for northern summer (MJJA). Associated correlation patterns of 45° N–45° S 200-mbar velocity potential (*lines*) and of outgoing long-wave radiation (OLR; *shading*). *Top*, q^2_χ and q^2_{OLR}; *middle*, q^1_χ and q^1_{OLR}; *bottom*, percentage of variance explained by POP coefficients. Units: velocity potential, $10^6 m^2 s^{-1}$; OLR, Wm^{-2}; variance, %

4.3 Meridional shift of analysis area

In another set of analyses, the area was shifted meridionally to 40° N or 40° S and yielded patterns and characteristic times similar to the A and B case (not shown). The variance of the POP coefficients, however, decreases with increasing latitudinal distance from the equator.

5 Associated correlation patterns: tropical velocity potential and OLR

5.1 Summary of the concept of associated correlation patterns

If a pair of POPs, p^1 and p^2, is identified in the key variable with time coefficients $z^1(t)$ and $z^2(t)$, the signal's appearance in another variable, say y, may be

identified by deriving *associated correlation patterns* q_y^1 and q_y^2, which are defined by

$$\langle \| y(t) - \hat{z}^1(t) q_y^1 - \hat{z}^2(t) q_y^2 \|^2 \rangle = \min$$

$\hat{z}^i(t)$ indicates a POP coefficient that is divided by its standard deviation (Storch et al. 1988). The normalization is introduced to obtain associated patterns with the same units as the analysed variable y. The associated correlation patterns is interpreted in a similar way to the POPs themselves: if the POPs perform one cycle, $\ldots \to p^1 - p^2 \to -p^1 \to p^2 \to p^1 \to \ldots$, the associated correlation patterns do the same

$$\ldots \to q_y^1 \to -q_y^2 \to -q_y^1 \to q_y^2 \to q_y^1 \to \ldots$$

The concept of associated correlation patterns allows one to separate the seasonal differences of the signal. To do so, the minimization is limited to dates from a particular season. We have done this for northern winter (NDJF) and summer (MJJA).

The associated correlation pattern analysis was carried out with two variables: velocity potential at 200 mbar in the 45° N–45° S belt – to check whether relevant information was disregarded when confining the POP analysis to the equator – and outgoing long-wave radiation (OLR). Since velocity potential is the output of an involved analysis scheme and OLR a directly measured quantity, the intercomparison of the patterns is an implicit consistency check.

5.2 Velocity potential and OLR patterns derived for all-year data

The patterns are shown in Fig. 6: velocity potential by isolines and OLR by different grades of shading. Not unexpectedly, the patterns of the velocity potential patterns along the equator are almost identical to the POPs. They are fairly symmetrical with respect to the equator – consistent with Section 4.3. q_χ^1 is shifted slightly northward, its extremes being located over the southern tip of India and in the Pacific ITCZ. In pattern q_χ^2, the Australian sector minimum is somewhat south of the equator. The variance explained by the two patterns is more than 50% almost everywhere along the equator, with maximum values of 79% in the Indian Ocean. Off the equator, the explained variance drops to about 40% at 45° N and 45° S.

The associated correlation OLR patterns appear well organized and explain up to 25% of the variance. The patterns are fairly symmetrical about the equator. The OLR and velocity potential patterns are mostly in phase. However, the largest anomalies of OLR and velocity potential are not at the same locations. In particular, the negative extreme of q_χ^1 is at about 120° W and that of q_{OLR}^1 at 170° E. The OLR anomalies are concentrated in those areas where, in the long term, mean precipitation is large – which is physically plausible.

In the 5° N–5° S/75° E–95° E box from which the area-averaged OLR time series (Fig. 4) was derived, velocity potential and OLR are not quite in phase. OLR leads velocity potential, so that the angle $\phi(90° \text{ E}) \approx 150°$ is slightly smaller than $\gamma(90° \text{ E}) \approx 170°$ (see Fig. 2).

5.3 Associated correlation patterns for northern winter

The associated correlation patterns of 200-mbar velocity potential and OLR in winter (NDJF) are displayed in Fig. 7. As expected, the winter patterns are shifted southward relative to the all-year patterns (Fig. 6).

In the eastern hemisphere a strong signal migrates eastward from the Indian Ocean across North Australia into the region of the SPCZ. In that area, the POPs account for more than 70% (30%) of the variance of velocity potential (OLR) (Fig. 7c). The western hemisphere appears less active: here, the velocity potential field is fairly flat and in the OLR no coherent structures are present. These results are consistent with the findings of Weickmann et al. (1985) and Madden (1986).

5.3 Associated correlation patterns for northern summer

The summer (MJJA) patterns (Fig. 8) are shifted northward relative to the all-year patterns (Fig. 6). In the velocity potential patterns, an eastward motion from the Asian monsoon area along the ITCZ to South America can be identified. In contrast to the winter situation, the patterns are well defined in the western hemisphere also. The maximum percentage of velocity potential variance represented by the POPs is 80% over the Indian Ocean and 60% over South America.

The centres of OLR action are in the northern hemisphere: northern Indian Ocean, India, the African and the Pacific ITCZ and northern South America. Maxima of explained variance are 20% in the Caribbean and at the Peruvian coast, and 25% in the Bay of Bengal. Over India, however, the amount of OLR variance which may be attributed to the 30- to 60-day oscillation is mostly less than 10%. In the Asian sector, the two patterns describe a northeastward propagation, and in the western hemisphere an eastward propagation.

These summer results are in accord with previously published results by Knutson et al. (1986) and Madden (1986).

6 Forecast experiments

6.1 Technique

The POP technique is naturally suited for predictions as it implies a forecast equation for the POP coefficients (Xu and Storch 1990, Penland 1989), namely

$$(z^1 + \imath z^2)(t+1) = \rho e^{-\frac{2\pi}{\mathscr{T}}} (z^1 + \imath z^2)(t)$$

where $\mathscr{T}$ denotes the rotation time (44 days in the present example) and ρ the damping rate (corresponding to 13 days in the present example). The equation describes the damped persistence of a trajectory in the complex

plane. Thus, in the framework of POP prediction, it is necessary only to identify the location in the complex state space of the system at a given time to predict future locations. For a limited time this prediction might be useful, but at longer lead times the built-in linearity of the POP analysis will result in a deterioration of the forecast skill.

There is a basic limitation of the POP forecasts: it is possible to predict only the regular changing phase of the oscillation and impossible to predict an intensification or a decay of the oscillation. However, a prediction of phase is potentially valuable even if the amplitude is not well predicted. Therefore, we predict the amplitude by persistence by setting $\rho = 1$ in the above prediction equation.

In view of the noisy character of the analysed variable, it is not sufficient to estimate the POP coefficients for a certain date and to use these as initial values. Instead, some "initialization" is necessary, e.g. the "time-averaging" approach or the "time-filtering" ansatz. The latter approach was introduced by Xu and Storch (1990): it operates with a one-sided digital filter suppressing variance on short time scales. We tested this approach, suppressing all variability shorter than 20 days. The results were essentially the same as those obtained with the "time-averaging" ansatz.

In the "time-averaging" ansatz, which is used throughout this paper, the POP coefficients are derived for the last few days. A 1-day POP forecast is made with the POP coefficients analysed at day -1, a 2-day forecast is made with the data of day -2 etc. A weighted average of the various forecasts and of the analysis at day 0 is used as an initial value. More weight is given to the recent information, and less to the older information. In this study, the POP coefficients of days 0 to -4 are used.

POP coefficients which are small and move irregularly in the 2-dimensional phase space indicate that the 30- to 60-day oscillation is not active and that the entire system is in a "quiet phase". In that case it would be reasonable not to rely on the formal POP forecast. Instead, the adequate POP forecast is that the system will stay in the "quiet phase".

6.2 *Case studies*

The forecasts are presented in the form of a "dial diagram showing the analysed evolutions of the POP coefficients before and after the forecast date, and the forecast itself. Ten randomly chosen cases are presented (Fig. 9 – for the details of the diagrams, see figure caption). They are all from the year 1985 and the forecast dates are about 30 days apart. The forecasts are made for 10 days in advance, which is about the *e*-folding time derived in the POP analysis. Note that all forecasts are from the verification interval, i.e. independent of the data the POP model is fitted to. Recall that the quality of the POP forecast has to be judged primarily by comparing the observed and predicted phases, rather than the amplitudes.

a) 22. 1. 1985. This case covers an early stage of the big event in late winter 1984/1985 (Fig. 3) and is a very useful forecast.
b) 23. 2. 1985. This forecast is successful for the first few days until the disruption of the oscillation's eastward propagation. The prediction is that the oscillation would continuously migrate eastward towards South America. In reality, however the oscillation changed direction after a few days, travelled westwards for a few days, and finally returned to its original orbit.
c) 26. 3. 1985. The big January/March 1985 event is over and the oscillation is weak. Accordingly, the forecast is that the amplitude will remain small. What actually happened was, however, that the oscillation recovered.
d) 25. 4. 1985. Quiet a realistic forecast.
e) 25. 5. 1989. The eastward propagation is heavily underpredicted.
f) 24. 6. 1985. A fairly successful forecast.
g) 6. 8. 1985. A good forecast – the POPs forecast the phase and cannot account for changes of the strength or for day-to-day variations.
h) 3. 9.1985. The situation prior to day 0 is inconsistent with the POP notion of a counterclockwise trajectory. This inconsistency is indicative that the system is in a quiet phase. The adequate – and correct – forecast is that the system will stay in the quiet phase.
i) 3. 10. 1985. The forecast is good even though the sudden intensification was not foreseen.
j) 2. 11. 1985. This forecast is quite good even though the phase propagation is underestimated.

To summarize subjectively: about half fo the forecasts seem to be skillful and one is wrong (c).

6.3 *Measures of skill*

To measure the quality of the POP forecasts, two measures of skill are used: the correlation skill $\mathscr{S}(\tau)$ and the "RMS" skill $\mathscr{R}(\tau)$

$$\mathscr{S}(\tau) = \frac{\langle \mathrm{a}_\tau^{\mathrm{T}}(t) \cdot \mathrm{b}(t) \rangle}{\sqrt{\langle \mathrm{a}_\tau(t)^2 \rangle \langle \mathrm{b}(t)^2 \rangle}}$$

$$\mathscr{R}(\tau) = \sqrt{\langle (\mathrm{a}_\tau(t) - \mathrm{b}(t))^2 \rangle}$$

Here, $\mathrm{a}_\tau(t)$ denotes a (bivariate) forecast issued at day t for τ days in advance. $\mathrm{b}(t)$ is a (bivariate) verifying quantity, in our case the POP coefficient time series itself. The brackets, $\langle . \rangle$, indicate ensemble averages. In our case, the ensemble consists of the forecasts made for each available day from May 1984 to April 1989.

The correlation skill $\mathscr{S}(\tau)$, being insensitive to amplitude errors, is an indicator of phase errors only. With respect to the amplitude, the POP forecast is a persistence forecast. Therefore, the correlation skill appears to be an adequate measure of skill of the POP method. The RMS error, $\mathscr{R}(\tau)$, is sensitive to both phase and amplitude errors. It may be anticipated, therefore, that the POP forecast appears less successful if measured in terms of RMS error.

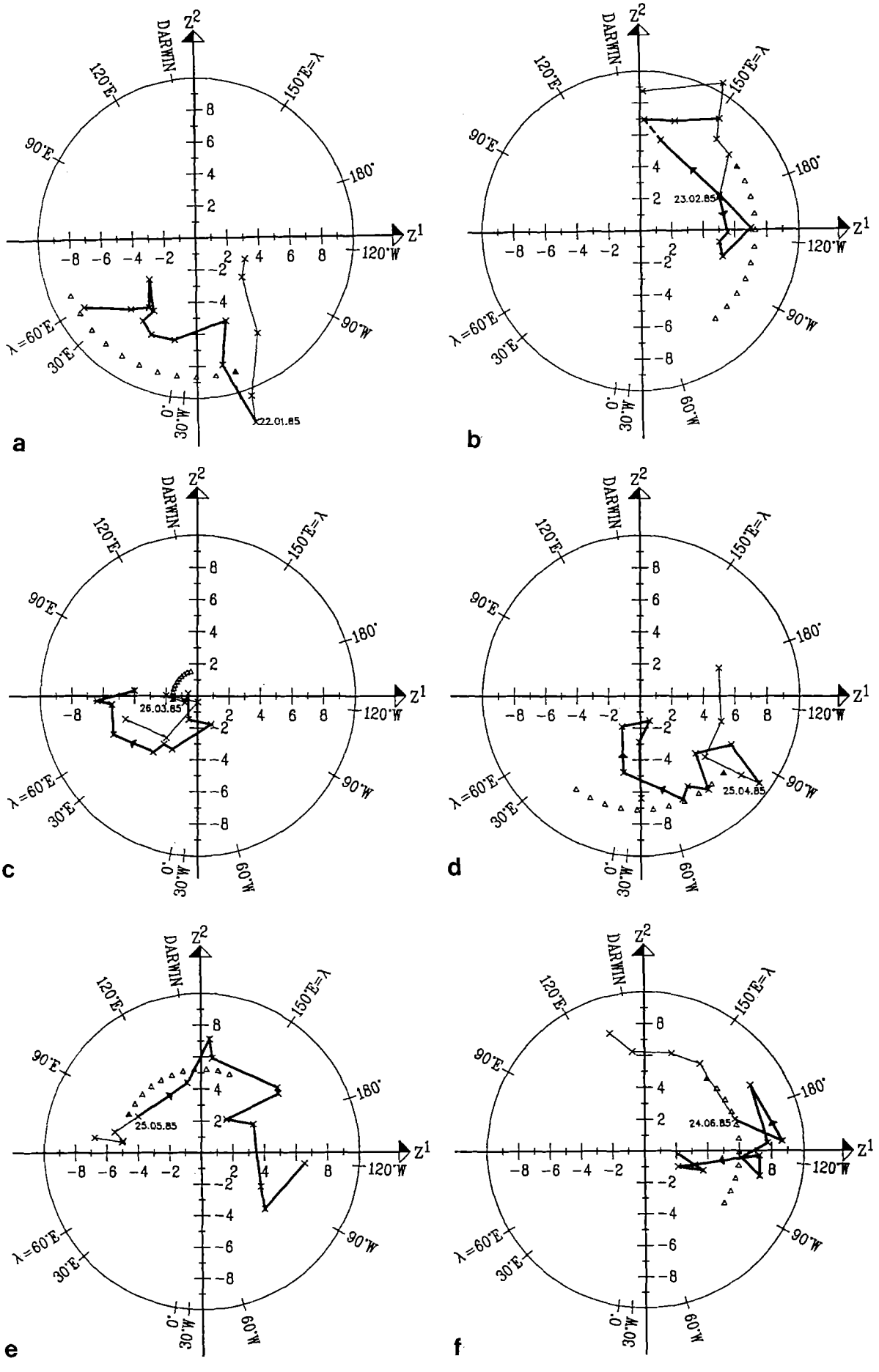
DARWIN
Z2
Z1
120°E
150°E=λ
90°E
180°
120°W
λ=60°E
30°E
0°
30°W
60°W
90°W
22.01.85
23.02.85
26.03.85
25.04.85
25.05.85
24.06.85
a
b
c
d
e
f

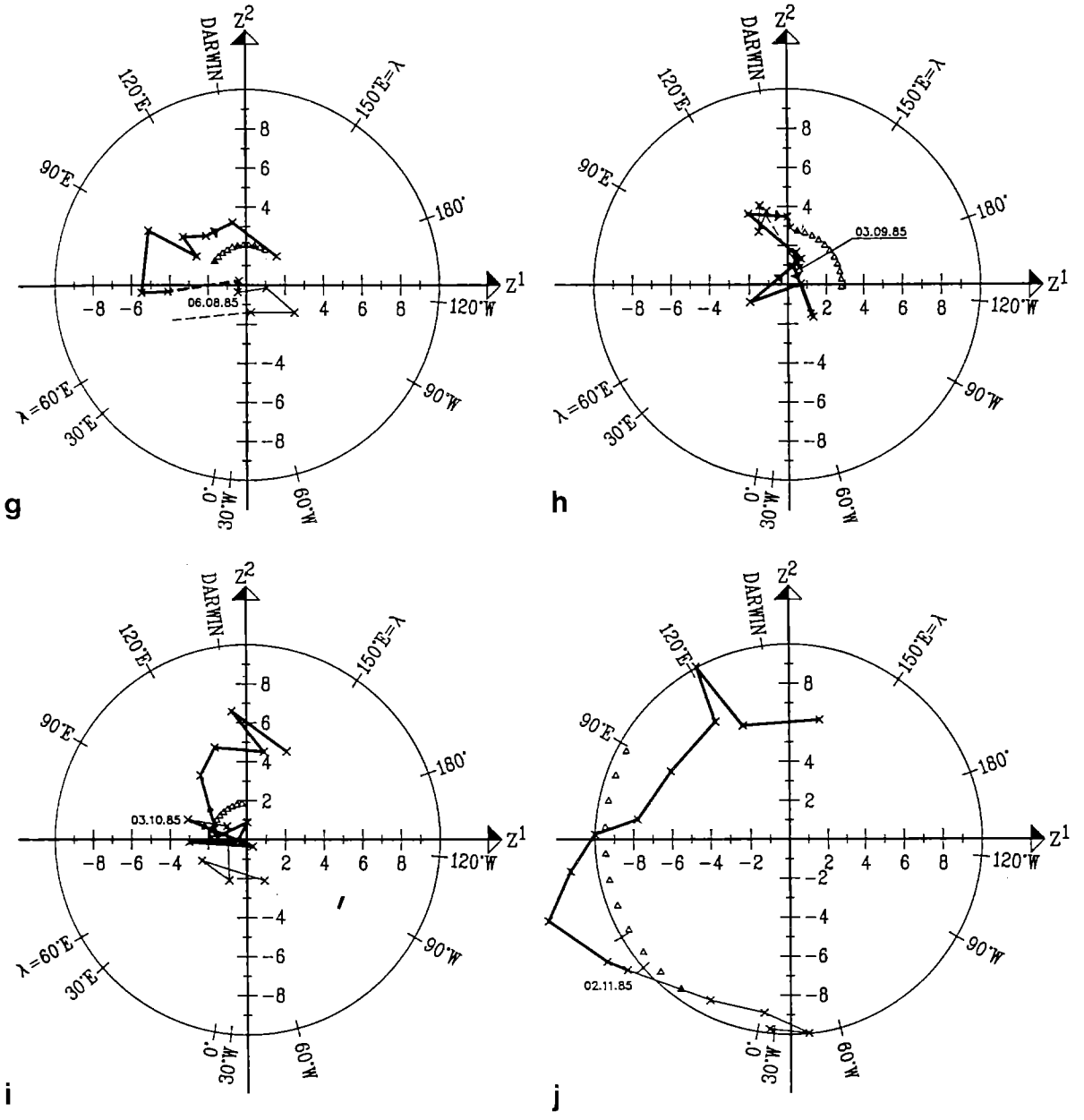

Fig. 9a–j. POP forecasts for 10 randomly chosen dates in 1985. The forecasts are made in the 2-dimensional POP coeffient plane with the x-asis representing the z^1 coefficient, and the y-axis the z^2 coefficient. The POP forecast model implies a clockwise rotation of the trajectory. The indicated geographic areas are ones that the minimum of the 200-mbar velocity potential passes over with given z^1 and z^2. See also Fig. 2. The *light continuous line* indicates the POP coefficients from day −4 day 0 and the *heavy continuous line* the POP coefficients found on days +1 to +10. The forecast itself is given by *triangles*. *Dashed lines* mark missing values in the observations. **a**: day 0 is 22. 1. 1985; **b**: 23. 2. 1985; **c**: 26. 3. 1985; **d**: 25. 4. 1984; **e**: 25. 5. 1985; **f**: 24. 6. 1985; **g**: 6. 8. 1985; **h**: 3. 9. 1985; **i**: 3. 10. 1985; **j**: 2. 11. 1985

To evaluate the merits of the POP forecast, its skill is compared with an even simpler forecast – the persistence forecast. Persistence is a fair choice as the POP forecast and the persistence may be seen next to each other in a hierarchy of forecast schemes of increasing complexity.

In the following subsection, the overall skill of the POP forecast is compared with that of persistence. It is reasonable to hypothesize that the forecast skill might depend on various factors such as season, strength of the signal and phase of the oscillation. In Subsections 6.5–6.7 the forecast skill is examined in this respect. Differently from most studies, the stratifications are made with respect to the state of the oscillation on the predicted day and not with respect to the state on the forecast day.

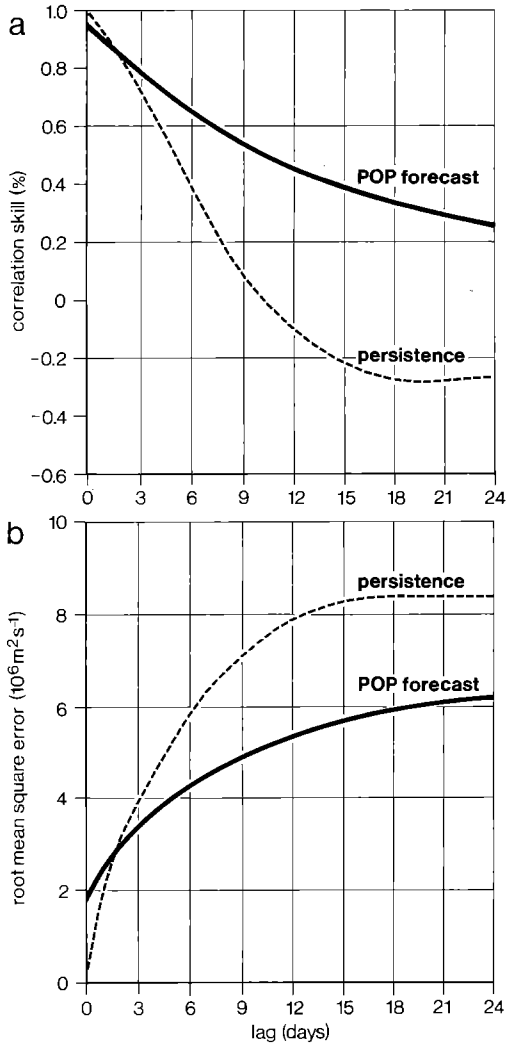

Fig. 10a, b. Measure of skill of the POP forecast (*solid*) and of persistence (*dashed*). The skills have been derived from daily forecast experiments for the entire period, May 1984 until April 1989. **a** Correlation skill, $\mathscr{S}(\tau)$: a "100%" indicates perfect skill, a "0" a useless forecast. **b** RMS skill, $\mathscr{R}(\tau)$

6.4 Skill scores for all data

The correlation skill, $\mathscr{S}(\tau)$, and the RMS error skill, $\mathscr{R}(\tau)$, derived from all forecast experiments, all dates, peristence and POP, are shown in Fig. 10. During the first 2 days the persistence appears more skillful than the POP forecast, but after this time the peristence forecast rapidly loses its skill. After about 20 days its skill has a negative extreme indicating the 30- to 60-day oscillatory behaviour of the oscillation. The RMS error skill reaches its saturation level of about $8.5 \cdot 10^6\ m^2 s^{-1}$ at day 18 (Fig. 10b).

The POP forecast correlation skill slowly decreases with time, yielding 60% after 7 days and 40% after 15 days. The increase of $\mathscr{R}(\tau)$ is considerably slower than in the case of the persistence. Even after 24 days, the saturation level is not yet reached.

It might be argued that the forecasts should be verified not against unfiltered POP coefficients but against low-pass filtered data – since it is the 30- to 60-day oscillation which is supposed to be predicted and not the day-to-day variations. We tried this, and used the mean of the last 3 days for the persistence. The results (not shown) are somewhat better than those shown in Fig. 10: the POP forecast was superior to the persistence forecast almost from the first day. The 60% (40%) line was passed after a lag of 10 (18) days.

6.5 Stratification with respect to seasons

We consider four seasons: DJF (December, January, February), MAM, JJA and SON. In terms of the correlation skill (Fig. 11a), the POP forecast is clearly superior to the persistence forecast in all four seasons. Both the persistence and the POP forecast score best in DJF, passing the 60% level after 5 days (persistence) and 11 days (POP forecast). The POP forecast has a minimum correlation skill in JJA.

Also in terms of the RMS skill score, the POP forecast is better than the persistence in all seasons (not shown). The POP forecast performs best in SON and worst in MAM. In the solstice seasons the RMS skill is about that of the all-year data.

6.6 Stratification with respect to strength of the signal

The strength of the signal is measured by the length $l(\mathbf{z}) = \sqrt{z_1^2 + z_2^2}$ of the bivariate POP coefficient $\mathbf{z} = (z_1, z_2)$. If μ_l denotes the mean length $l(\mathbf{z})$, the skills are derived for all $\mathbf{z}$ with $l(\mathbf{z}) \geq 9, \mu_l, \frac{3}{2}\mu_l, 2\mu_l$.

Interestingly, the persistence correlation skill is the same for $l(\mathbf{z}) \geq 0, \mu_l, \frac{3}{2}\mu_l$ (Fig. 11b). For $l(\mathbf{z}) \geq 2\mu_l$, however, the skill curve is somewhat irregular, indicating sampling problems. The sample size for $l(\mathbf{z}) \geq 2\mu_l$ is only 29, and not all samples are independent of each other. For the other three cases, $l(\mathbf{z}) \geq 0, \mu_l, \frac{3}{2}\mu_l$, the sample sizes are 1750, 661 and 179. We conclude that the correlation skill of the peristence is independent of the strength of the signal.

The correlation skill of the POP forecast increases with the strength of the signal (Fig. 11b). The 60% level is passed after 7 days for all data, after 10 days if $l(\mathbf{z}) \geq \mu_l$, after 12 days if $l(\mathbf{z}) \geq \frac{3}{2}\mu_l$, and after 21 days if $l(\mathbf{z}) \geq 2\mu_l$. The last estimate, however, is probably contaminated by sampling uncertainties.

As expected, the RMS skill of the persistence forecast and the POP forecast increase with the strength of the signal (not shown). Interestingly, however, the difference between the peristence and the POP forecast also increases with the strength of the signal. The differences in $\mathscr{R}$(9 days) are about $2 \times 10^6\ m^2 s^{-1}$ for $l(\mathbf{z}) \geq 0$, $3 \times 10^6\ m^2 s^{-1}$ for $l(\mathbf{z}) \geq \mu_l$, $4 \times 10^6\ m^2 s^{-1}$ for $l(\mathbf{z}) \geq \frac{3}{2}\mu_l$ and $5 \times 10^6\ m^2 s^{-1}$ for $l(\mathbf{z}) \geq 2\mu_l$ (the last estimate is questionable).

6.7 Stratification with respect to phase of the oscillation

The correlation skills for the four equatorial 90° sectors (see Section 4) (A) 90° W–0°, (B) 180°–90° W, (C)

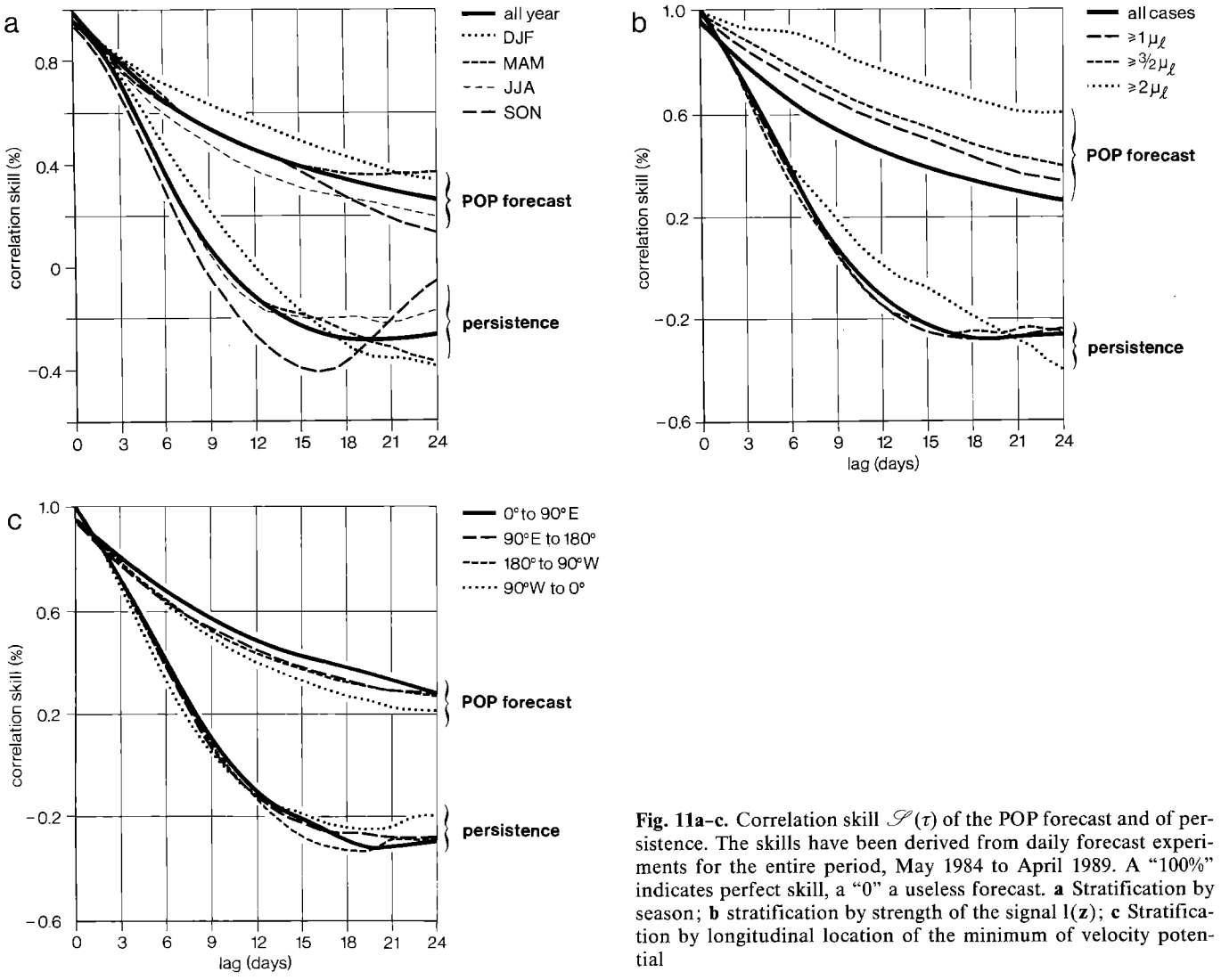

Fig. 11a–c. Correlation skill $\mathscr{S}(\tau)$ of the POP forecast and of persistence. The skills have been derived from daily forecast experiments for the entire period, May 1984 to April 1989. A "100%" indicates perfect skill, a "0" a useless forecast. **a** Stratification by season; **b** stratification by strength of the signal $l(\mathbf{z})$; **c** Stratification by longitudinal location of the minimum of velocity potential

90° E–180° and (D) 0°–90° E are shown in Fig. 11c. Having found in Section 4.2 that the signal is best developed in the eastern hemisphere, it is not surprising to find maximum correlation skill along that part of the equator. In the 90° W–0° sector the skills are worst.

7 Summary and outlook

Without applying any time filter, the POP analysis leads to the definition of an index of the 30- to 60-day oscillation. This index is highly correlated with a local OLR time series and it is possible to derive essential properties of the oscillation, e.g. the meridional displacement of its track from summer to winter, by exploiting the index.

The characteristics of the index do not depend on the choice of analysis period or analysis area. If the entire 5-year data set is analysed, the same index is obtained as from the 2-year interval used here. The analysis of 90° longitude sectors along the equator also leads to essentially the same index. The signal appears most clearly in the eastern hemisphere, i.e. in the 0°–90° E and 90°–180° sectors.

The POP index of the 30- to 60-day oscillation is predictable for several days. The POP forecast scheme, which is considerably better than persistence, scores a correlation skill of more than 60% during the first 7 forecast days. The POP forecast seems to be most skillful in northern winter, and in the eastern hemisphere, provided that the signal is strong.

The existence of an easy-to-handle index of the 30- to 60-day oscillation allows a number of questions related to the oscillation to be studied in a relatively straightforward manner. For instance, changes of the global atmospheric energetics and of the general circulation connected with the course of the oscillation may easily be inferred from daily analyses by applying the "associated correlation pattern" analysis. Another example is the possible relationship between the state of the oscillation and extratropical predictability.

Acknowledgements. The main part of this work was done during a visit to the Cooperative Institute for Research in Environmental

Sciences (CIRES) in Boulder (Colorado). We wish to thank Rol Madden for his inspiration and George Kiladis, Klaus Weickmann, Brant Liebmann and Dierk Schriever for helpful discussions and technical support. Marion Grunert and Mrs. Lewandowski prepared the diagrams. The Manuscript Correction Service of Peter and Diana Wright helped with the language.

References

Hartmann D, Michelsen ML (1989) Intraseasonal perodicities in Indian rainfall. J Atmos Sci 46:2838–2862

Hasselmann K (1988) PIPs and POPs: The reduction of complex dynamical systems using Principal Interaction and Oscillation Patterns. J Geophys Res 93:11015–11021

Huang H-J, Vincent DG (1988) Active and inactive phases of the South Pacific Convergence Zone and changes in global circulation patterns: a case study. Beitr Phys Atmos 61:123–134

Knuson TR, Weickmann KM (1987) 30–60 day atmospheric oscillations: composite life cycles of convection and circulation anomalies. Mon Weather Rev 115:1407–1436

Knutson TR, Weickmann KM, Kutzbach JE (1986) Global-scale intraseasonal oscillations of outgoing longwave radiation and 250 mb zonal wind during Northern Hemisphere summer. Mon Weather Rev 114:605–623

Latif M, Villwock A (1989) Interannual variability in the tropical Pacific as simulated in coupled ocean-atmosphere models. J Marine Systems (in press)

Lau K-M, Chan PH (1985) Aspects of the 40–50 day oscillation during northern winter as inferred from outgoing long wave radiation. Mon Weather Rev 113:1889–1909

Liebmann B, Chelliah M, van den Dool HM (1989) Persistence of outgoing long wave radiation anomalies in the tropics. Mon Weather Rev 117:670–679

Madden RA (1986) Seasonal variations of the 30–60 day oscillation in the tropics. J Atmos Sci 43:3138–3158

Madden RA (1987) Relationships between changes in the length of day and the 40- to 50-day oscillation in the tropics. J Geophys Res 92:8391–8399

Madden RA (1988) Large intraseasonal variations in wind stress over the tropical Pacific. J Geophys Res 93:5333–5340

Madden RA, Julian PR (1972) Description of global-scale circulation cells in the tropics with a 40–50 day period. J Atmos Sci 24:1109–1123

McBride JL (1987) The Australian summer monsoon. In: Chang CP, Krishnamurti TN (eds) Monsoon meteorology. Oxford University Press, pp 203–231

Penland C (1989) Random forcing and forecasting using Principal Oscillation Pattern analysis. Mon Weather Rev 117:2165–2185

Rosen RD, Salstein DA (1983) Variations in atmospheric angular momentum on global and regional scales and the length of day. J Geophys Res 88:5451–5470

Storch H von, Bruns T, Fischer-Bruns I, Hasselmann K (1988) Principal Oscillation Pattern analysis of the 30-to 60-day oscillation in a general circulation model equatorial troposphere. J Geophys Res 93:11022–11036

Storch H von, Weese U, Xu J (1990) Simultaneous analysis of space-time variability: Principal Oscillation Patterns and Principal Interaction Patterns with applications to the Southern Oscillation. Z Meteor 40:99–103

Trenberth KE, Olson JG (1988) Evaluation of NMC global analyses: 1979–1987, NCAR Technical Note NCAR/TN-299+STR

Weickmann KM, Lussky GR, Kutzbach JE (1985) Intraseasonal (30–60 day) fluctuations of outgoing longwave radiation and 250 mb streamfunction during northern winter. Mon Weather Rev 113:943–961

Xu J, Storch H von (1990) "Principal Oscillation Pattern"-prediction of the state of ENSO. J Climate (in press)